Spatial Properties of Entangled Two-Photon Absorption

D. Tabakaev, A. Djorović, L. La Volpe, G. Gaulier, S. Ghosh, L. Bonacina, J.-P. Wolf, H. Zbinden, and R. T. Thew
Département de Physique Appliquée, Université de Genève, 1211 Genève, Switzerland

(Received 6 June 2022; revised 22 August 2022; accepted 30 September 2022; published 24 October 2022)

We experimentally study entangled two-photon absorption in rhodamine 6G as a function of the spatial properties of a high flux of broadband entangled photon pairs. We first demonstrate a key signature dependence of the entangled two-photon absorption rate on the type of entangled pair flux attenuation: linear, when the laser pump power is attenuated, and quadratic, when the pair flux itself experiences linear loss. We then perform a fluorescence-based Z-scan measurement to study the influence of beam waist size on the entangled two-photon absorption process and compare this to classical single- and two-photon absorption processes. We demonstrate that the entangled two-photon absorption shares a beam waist dependence similar to that of classical two-photon absorption. This result presents an additional argument for the wide range of contrasting values of quoted entangled two-photon absorption cross sections of dyes in literature.

DOI: 10.1103/PhysRevLett.129.183601

Introduction.—Two-photon excitation microscopy and spectroscopy techniques are broadly required in both fundamental research and applications due to the relatively high penetration depths and the possibility of 3D slicing [1,2]. However, these techniques also suffer from fundamental disadvantages, such as low absorption cross sections [3–5]. The latter is due to the quadratic dependence of an absorption rate on the photon flux, which is typically compensated by the use of pulsed lasers. Theory predicts [6–10] that entangled two-photon absorption (ETPA) is capable of mitigating the small absorption cross-section problem as the photon pairs behave as single quantum objects, which results in a linear rate dependence on the input photon-pair flux, leading to much lower excitation fluxes to obtain the signal. This feature has been observed by several groups experimentally [11–17], but only the photon pair rate incident to the sample was controlled and varied in previous studies.

According to theory [6], the two-photon absorption (TPA) rate under continuous-wave laser excitation rate R_{laser} [s^{-1}] can be written as

$$R_{\text{TPA}} = C\,A l \delta \frac{R_{\text{laser}}^2}{A^2} \tag{1}$$

where, C [cm^{-3}] is the concentration, l [cm] the sample length, A [cm^2] the beam waist area, and δ [GM] the TPA cross section. It is clear that the resulting TPA rate scales as $(1/A)$. Following the same logic, the expression for the ETPA rate under continuous-wave photon pair excitation rate R_{pair} [pairs/s] reads as [6,17]

$$R_{\text{ETPA}} = C\,A l \frac{\delta}{A_e T} \frac{R_{\text{pair}}}{A}, \tag{2}$$

where A_e [cm^2] is the so-called "entanglement area" [18] and T is the coherence time of a pair, such that $\sigma_e = (\delta/A_e T)$ is the ETPA cross section. The entanglement area is the surface within which a photon of the pair can be found, defined by the uncertainty of its production position and angle. The diameter of this area is defined by the transverse coherence function of the pairs [19]. In the experimentally relevant case, multiple pairs are produced by spontaneous down-conversion (SPDC), and then focused to the sample consisting of multiple molecules or atoms. Typically, the focal spot size in the sample is much smaller than the FWHM of the transverse coherence function of the pairs, which means that much more than 50% of pairs are capable of producing a "coincidence"—or a two-photon absorption event—in the molecules which are present within the beam focal spot size. Intuitively this comparison shows us that the focal spot size in the sample is small enough to guarantee that the spatial transverse separation between the photons of the same pair is small as well, so the vast majority of the photons are "seen" and absorbed by molecules as pairs. Under these conditions it is fair to assume that $A_e = A$ and that the ETPA rate depends on the area of the beam waist in the same manner as the TPA rate.

The conventional way of studying nonlinear optical properties, i.e., absorption and refraction, of a sample, is to use the Z-scan technique [20]. In a classical Z-scan measurement, a thin sample is placed on a translation stage and exposed to a focused laser beam, whose photons can be

absorbed in a nonlinear process only. Information about the sample properties is derived from the laser power dependence on the translation stage position, i.e., dependence of laser beam losses as the focal spot size of the beam is varied. This method can be used to assess ETPA as well, but instead of laser power, the photon pair coincidence detection rate is needed, which is conventionally obtained using time-correlated single photon counting techniques. However, this is extremely challenging and misalignment of the entangled photon pair beam due to the sample movement can result in variations of coupling efficiency of the photons after passing through the sample and before the detectors, resulting in a complicated problem of distinguishing coupling losses from pair absorption events [14,16,21].

In this Letter, we investigate the spatial properties of ETPA by comparing the resultant fluorescence signals in an epiconfiguration with those induced by single-photon absorption (SPA) and TPA. We conclude with a discussion on the implication for our understanding of ETPA and its applications in microscopy and spectroscopy.

Experimental setup.—Figure 1 shows a schematic of the experimental setup. The photon pairs are generated by pumping a 2 cm periodically poled Lithium niobate (PPLN) crystal (Covesion MSHG1064-0.5-20, 0.5×0.5 mm^2 aperture) with 2.5 W from a 532 nm continuous-wave laser with less than 5 MHz linewidth (Coherent Verdi V5) focused down to a 70 μm beam waist by 200-mm (Thorlabs LBF-254-200-A) and 40-mm (Thorlabs LBF-254-040-A) lenses. The laser power is controlled by a 10-cm Glan-Taylor Polarizer (Thorlabs GT-10-A) and half-wave plate. The PPLN crystal is temperature phase matched to produce type-0 degenerate SPDC pairs with a bandwidth of about 30 nm, centered at 1064 nm, corresponding to 140 fs coherence time. The 532 nm pump laser with 0.2 μs coherence time is blocked by three long pass interference filters (IF_L) (Thorlabs FELH0750, FELH0900 and FELH1050). The photon pair source was characterized

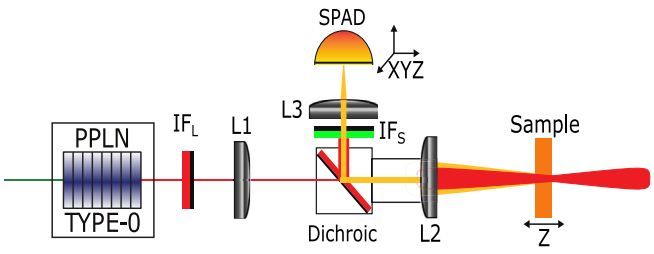

FIG. 1. Epifluorescence setup schematic: PPLN—periodically poled lithium niobate crystal, pumped by 532 nm laser; IF_L—set of long-pass interference filters; L1—pair collimating lens; Dichroic—dichroic mirror, transparent to IR and reflective to visible light; L2—pair focusing and fluorescence collecting lens; Sample—cell with liquid Rh6G solution; Z—translation stage; IF_S—short-pass interference filter; L3—fluorescence focusing lens; SPAD—single-photon avalanche diode.

similarly to [17]: photon pairs were coupled to a single-mode fiber beam splitter and sent to two single-photon detectors (ID Quantique ID201 and ID220), connected to a time-to-digital converter. By performing time-correlated single-photon counting, we found the number of coincidence detections per mW of pump power. Scaling this value to higher pump power and measuring the SPDC beam power with a power meter (Thorlabs S120C) and the same set of long-pass filters we verified that it scales linearly with the laser pump power. The maximum SPDC power was about 0.16 μW ($\sim 8.7 \times 10^{11}$ s^{-1}). Taking into account the laser and SPDC bandwidth, the number of SPDC temporal modes was about 6.3×10^6, with approximately 0.12 photons per mode along the same lines as in [22].

SPDC pairs are collimated by a 10 cm lens (L1, Thorlabs LBF254-100-C) and, after passing the dichroic mirror (Thorlabs DMLP650R), pairs are focused to the sample mounted on the translation stage (Thorlabs MTS25/M) by a 3 mm lens (L2, Thorlabs C330TMD-A). The fluorescence from the sample is collected by the same lens L2, before being reflected by a dichroic mirror through three short-pass filters (Thorlabs FESH0650) and then focused by an 11 mm lens (L3, Thorlabs A397TM-A) to a single-photon avalanche diode (SPAD, ID Quantique ID120, $\sim$200 dark counts s^{-1}) mounted on a three-axis translation stage.

ETPA signature.—While ETPA is more efficient with respect to photon flux than TPA, the signal-to-noise ratio (SNR) of experiments relying on entangled photon sources is typically low. It is therefore important that the detected signals are indeed produced by the ETPA process and not arising from pump leakage, hot-band single-photon absorption [23], or any other single-photon process. The risk of this misattribution comes from the indistinguishability of fluorescence signals, produced by these events that would have the same type of (linear) dependence on the input flux.

We can distinguish these two possible contributions by comparing the fluorescence count rates while attenuating the pump or the photon pair fluxes [22]. Using the setup from Fig. 1, we focused SPDC pairs into a thin home-built cell with 5 mM liquid solution of Rh6G in ethanol with a lens of 3 mm focal length. In the first set of measurements, we controlled the power of the pump laser with a half-wave plate and Glan-Taylor polarizer while detecting the ETPA-induced Rh6G fluorescence for different *pump* attenuations. In the second set of measurements, we increasingly attenuated the SPDC flux by a set of ND filters, and recorded the signal for different *pair* attenuations. The same measurements were performed with the laser turned off to determine the background level, which is dominated by the detector dark counts. The results are shown in Fig. 2. The fitting was performed by a least-squares method, resulting in the coefficient of determination $R^2 = 0.997$ for the linear fit and root mean squared error (RMSE) of 0.12 for the quadratic one. A linear dependence in the case of laser beam attenuation, and quadratic in the case of

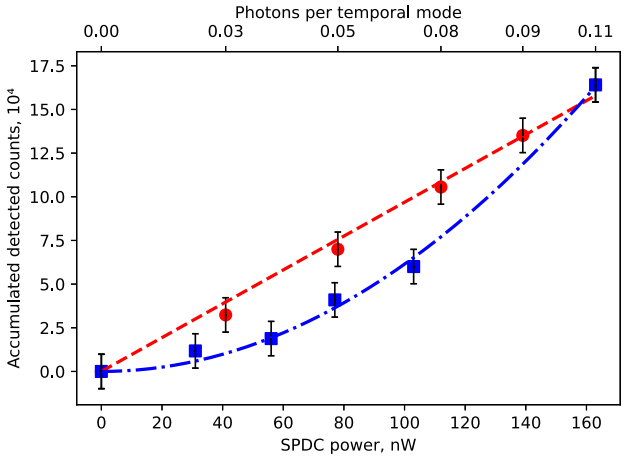

FIG. 2. ETPA-induced fluorescence counts as a function of laser pump power attenuation (red circles) and SPDC flux attenuation (blue squares), concentration of Rh6G in ethanol is 5 mM. Each point is an integration of detector counts over 2×10^4 s, 4.3×10^6 accumulated dark counts subtracted. Error bars are standard deviations over the set of measurements. The red dashed line corresponds to a linear fit and the blue dash-dotted line to a quadratic fit of the experimental data.

SPDC beam attenuation, confirmed that the measured signal was due to ETPA and not caused by direct detection of scattered pump, down-converted photons, or single-photon absorption of any type [23]. It also constitutes one of the most robust demonstrations of genuine ETPA [24–26].

Epifluorescence Z scan.—To perform the fluorescence-based Z scan measurement, the sample is mounted on a translation stage and exposed to the focused SPDC beam. Measuring fluorescence instead of beam attenuation allows us to neglect possible misalignment changing the photon coupling of the entangled pair beam relative to the sample position at the cost of a more challenging alignment of the fluorescence collection optics and single-photon detector position. This choice also increases pump filtering requirements so as to clearly see the fluorescence. Each measurement consists of the integration of fluorescence detections from the home-built cell with a 5 mM liquid Rh6G ethanol solution, which is scanned through the excitation beam's focal point.

In the first instance we use a 1064 nm continuous-wave laser (Coherent Prometheus) as a source of excitation, which is focused down to a 1.5 μm waist to measure classical TPA-induced fluorescence as a reference. Figure 3 shows the results of this scan where the full width at half maximum (FWHM) of the measured axial profile was about 120 μm. This value corresponds well to the 126 μm thickness of the sample that was measured using a commercial multiphoton microscope.

Similarly, we measured the SPA response by focusing a 532 nm laser down to a 4.4 μm waist setting a long-pass filter with a cutoff at 550 nm (Thorlabs FELH0550) to ensure only fluorescence photons are detected and any scattered light is blocked.

We finally injected the entangled photon pairs at maximum laser pump power (about 8.7×10^{11} s^{-1}, 0.16 μW) and focused them down to a 4.5 μm waist on the cell with liquid Rh6G solution. The signal (10 counts/s) obtained by replacing the Rh6G sample by pure ethanol was subtracted for background correction. During the scanning we consider an extreme case for the maximum beam size during this measurement of 30 μm and assume that $A_e = A$ remains valid.

In Fig. 3 we see all three measurement results. It is clear that the FWHM of the SPDC Z-scan profile lies between the widths of the two classical references obtained in the same geometry. To compare the results we first modeled the fluorescence rate which can be detected when using an undepleted Gaussian beam for TPA and SPA taking into account the 1064 nm and 532 nm laser beam parameters, respectively [27]. We start from calculating the effective fluorescence collection waists w_z and $w_{z\mathrm{TP}}$ in case of single- and two-photon absorption, respectively,

$$w_z = \sqrt{\frac{w_0^2 + \frac{\lambda^2}{4\pi^4 \mathrm{NA}^2} + 2w_d^2}{\frac{\lambda^2}{(4\pi^4 w_0^2)+\mathrm{NA}^2}}} \tag{3}$$

$$w_{z\mathrm{TP}} = \sqrt{\frac{w_0^2 + \frac{\lambda_{\mathrm{TP}}^2}{2\pi^4 \mathrm{NA}^2} + 2w_d^2}{\frac{\lambda_{\mathrm{TP}}^2}{(4\pi^4 w_0^2)+2\mathrm{NA}^2}}}, \tag{4}$$

where w_0 is a beam waist size at the focus, NA = 0.7 is the numerical aperture of the excitation and collection lens L2, λ and λ_{TP} are excitation wavelengths for single- and two-photon absorption cases, respectively, w_d is the fluorescence beam waist on the detector (detector diameter is 500 μm). We then put these values into the expressions describing the normalized fluorescence detection rate for SPA and TPA given by

$$R^{\mathrm{SPA}}(z) = \arctan\left(\frac{z+d}{w_z}\right) - \arctan\left(\frac{z-d}{w_z}\right) \tag{5}$$

$$R^{\mathrm{TPA}}(z) = w_{z\mathrm{TP}}\left[\arctan\left(\frac{z+d}{z_R}\right) - \arctan\left(\frac{z-d}{z_R}\right)\right] - z_R\left[\arctan\left(\frac{z+d}{w_{z\mathrm{TP}}}\right) - \arctan\left(\frac{z-d}{w_{z\mathrm{TP}}}\right)\right]. \tag{6}$$

Here z is the displacement of the sample relative to the beam focus, d is the sample thickness, and z_R is the Rayleigh range. To fit the experimental data on Fig. 3, a sample thickness d, the detector size, and focal spot size w_0 were left as free parameters and a least square optimization algorithm used the measured values of these parameters as

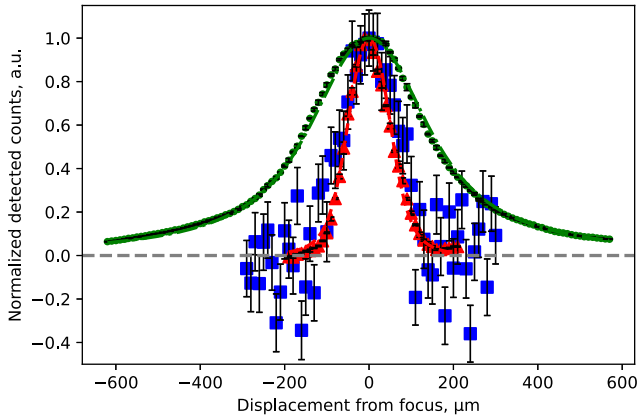

FIG. 3. Normalized fluorescence detection rate from a liquid 5 mM Rh6G ethanol solution as a function of translation stage displacement from the focus in the epifluorescence scheme. The fluorescence is induced by 532 nm laser photons (green circles); SPDC pairs (blue squares), and 1064 nm laser photons (red triangles). The SPDC-induced fluorescence data points are an average of 100 measurements of 1 s each and the laser induced are an average of 5 measurements of 1 s each, measured at 10 μm displacement intervals. The red dashed line is the model of the TPA for a Gaussian 1064 nm laser beam (6). The green dash-dotted line is the model of SPA for a 532 nm beam (5). Error bars are Monte Carlo propagated standard deviations. The sizes of error bars for SPA and TPA data points are smaller than the data points.

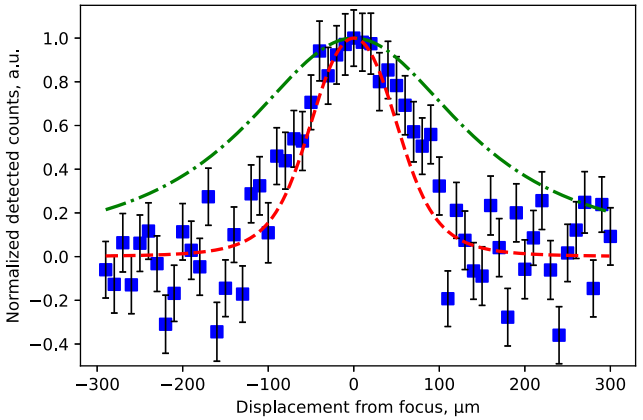

FIG. 4. Normalized fluorescence detection rate from a liquid 5 mM Rh6G ethanol solution as a function of translation stage displacement from the focus in the epifluorescence scheme under the SPDC excitation (blue squares), and models of fluorescence rate under single- (red dashed line) and two-photon excitation (green dash-dot line), described in Eqs. (5) and (6).

a starting guess. The resulting fits of the measured fluorescence rates yield a RMSE of 0.017 in the SPA case and 0.035 in the TPA case.

To fit the ETPA data, we fixed the excitation wavelength at the central wavelength of SPDC pairs, at 1064 nm, and used the parameters obtained from the fitting of classical references: $d = 120$ vs 126 μm measured, $w_0 = 4.65$ vs 4.4 μm measured, and $w_d = 94$ μm which was not measured but is much smaller than the detector diameter of 500 μm. The result is demonstrated in the Fig 4: when fitted by a model of the fluorescence rate produced under the single-photon excitation RMSE is 0.383, while the TPA model fits with a RMSE of 0.171.

Discussion.—In Fig. 2 we demonstrated one of the clearest signatures of ETPA both highlighting linearity of its rate as a function of SPDC rate and also that experimentally the fluorescence is induced by the pairs and not from experimental artifacts. This provides the baseline to unambiguously study the spatial characteristics in the epidetection configuration that is of relevance in the context of microscopy.

Using the fluorescence-based Z scan we demonstrated the similarity between shapes and widths of TPA and ETPA spatial profiles in a regime where we assume the entanglement area A_e is equal to the focal spot area of the SPDC beam. It could be interesting to investigate this assumption further by considering the joint spatiotemporal correlation function [28] and verify the scaling of the excitation volume, e.g., in a regime where the entanglement area is smaller than the focal spot. We further reinforced our analysis by modeling the fluorescence rate under single- and two-photon excitation and confirmed that despite the fact that ETPA rate scales linearly as a function of the excitation photon pair rate, its spatial properties follow a TPA-like behavior.

The spatial dependence of the ETPA rate has broader implications in studies of ETPA processes. Consistent and standardized reporting of ETPA rate values is critical to untangling the many contrasting reported values of ETPA cross sections. Our results suggest that reporting an ETPA cross section, σ_e, value for a given system is insufficient. Because of this dependence on spatial and temporal properties of a pair source, we believe that $\sigma_e \times A \times T$, where A is the cross section of the SPDC beam at focus and T is its coherence time, is a more pertinent choice of value to use when comparing different optical systems and experiments.

For example, the line in Fig. 2 corresponds to σ_e on the order of $\sim(5 \pm 1) \times 10^{-22}$ cm^2, which corresponds up to an order of magnitude to the previously obtained value for a Rh6G study [17], and combined with the beam waist area and coherence time of SPDC beam $\sigma_e \times A_e \times T_e \approx 4.4 \times 10^{-41}$ cm^4 s, which, according to the relation between classical and entangled TPA cross sections [6], should be the value of the Rh6G TPA cross section on the order of $10^{-47} - 10^{-49}$ cm^4 s [5,29]. Taking into account uncertainties which are present in the measurements of these four values, and the maximum quantum enhancement bound of 10^5 stated in [24], we can see that the TPA cross section calculated from our results is still 1–2 orders of magnitude bigger than the one measured experimentally.

These results hopefully encourage others working on this phenomenon, as clearly, further studies are needed to not only reproduce them but overcome the extremely low ETPA-induced signals and challenging SNR. This could be accomplished with better collection optics and detection scheme—including the impact of spatial aberrations or the quality of the SPDC focus, as well as better understanding of the entangled photon pair sources, and the light-matter interaction itself.

We acknowledge support from the Swiss National Science Foundation through the Sinergia Grant No. CRSII5-170981. We also wish to thank Ralph Jimenez, Martin Stevens, and Michael Raymer for many fruitful discussions and insights.

[1] S. Szoke, H. Liu, B. P. Hickam, M. He, and S. K. Cushing, Entangled light–matter interactions and spectroscopy, J. Mater. Chem. C **8**, 10732 (2020).

[2] M. F. García, R. J. Echeverría, M. Moll, R. M. Santos, R. P. Pinto, I. Vila, and M. Wiehe, High resolution 3d characterization of silicon detectors using a two photon absorption transient current technique, Nucl. Instrum. Methods Phys. Res., Sect. A **958**, 162865 (2020).

[3] H. B. Bebb and A. Gold, Multiphoton ionization of hydrogen and rare-gas atoms, Phys. Rev. **143**, 1 (1966).

[4] B. Mollow, Two-photon absorption and field correlation functions, Phys. Rev. **175**, 1555 (1968).

[5] P. Sperber and A. Penzkofer, S 0-s n two-photon absorption dynamics of rhodamine dyes, Opt. Quantum Electron. **18**, 381 (1986).

[6] H.-B. Fei, B. M. Jost, S. Popescu, B. E. A. Saleh, and M. C. Teich, Entanglement-Induced Two-Photon Transparency, Phys. Rev. Lett. **78**, 1679 (1997).

[7] B. Dayan, Theory of two-photon interactions with broadband down-converted light and entangled photons, Phys. Rev. A **76**, 043813 (2007).

[8] F. Schlawin, Entangled photon spectroscopy, J. Phys. B **50**, 203001 (2017).

[9] K. E. Dorfman, F. Schlawin, and S. Mukamel, Nonlinear optical signals and spectroscopy with quantum light, Rev. Mod. Phys. **88**, 045008 (2016).

[10] M. G. Raymer, T. Landes, M. Allgaier, S. Merkouche, B. J. Smith, and A. H. Marcus, How large is the quantum enhancement of two-photon absorption by time-frequency entanglement of photon pairs?, Optica **8**, 757 (2021).

[11] D.-I. Lee and T. Goodson, Entangled photon absorption in an organic porphyrin dendrimer, J. Phys. Chem. B **110**, 25582 (2006).

[12] M. R. Harpham, O. Süzer, C.-Q. Ma, P. Bäuerle, and T. Goodson III, Thiophene dendrimers as entangled photon sensor materials, J. Am. Chem. Soc. **131**, 973 (2009).

[13] L. Upton, M. Harpham, O. Suzer, M. Richter, S. Mukamel, and T. Goodson III, Optically excited entangled states in organic molecules illuminate the dark, J. Phys. Chem. Lett. **4**, 2046 (2013).

[14] J. P. Villabona-Monsalve, O. Calderon-Losada, M. Nuñez Portela, and A. Valencia, Entangled two photon absorption cross section on the 808 nm region for the common dyes zinc tetraphenylporphyrin and rhodamine b, J. Phys. Chem. A **121**, 7869 (2017).

[15] O. Varnavski, B. Pinsky, and T. Goodson III, Entangled photon excited fluorescence in organic materials: An ultrafast coincidence detector, J. Phys. Chem. Lett. **8**, 388 (2017).

[16] J. P. Villabona-Monsalve, R. K. Burdick, and T. Goodson III, Measurements of entangled two-photon absorption in organic molecules with CW-pumped type-I spontaneous parametric down-conversion, J. Phys. Chem. C **124**, 24526 (2020).

[17] D. Tabakaev, M. Montagnese, G. Haack, L. Bonacina, J.-P. Wolf, H. Zbinden, and R. T. Thew, Energy-time-entangled two-photon molecular absorption, Phys. Rev. A **103**, 033701 (2021).

[18] B. M. Jost, A. V. Sergienko, A. F. Abouraddy, B. E. Saleh, and M. C. Teich, Spatial correlations of spontaneously down-converted photon pairs detected with a single-photon-sensitive ccd camera, Opt. Express **3**, 81 (1998).

[19] J. Schneeloch and J. C. Howell, Introduction to the transverse spatial correlations in spontaneous parametric down-conversion through the biphoton birth zone, J. Opt. **18**, 053501 (2016).

[20] M. Sheik-Bahae, A. A. Said, T.-H. Wei, D. J. Hagan, and E. W. Van Stryland, Sensitive measurement of optical nonlinearities using a single beam, IEEE J. Quantum Electron. **26**, 760 (1990).

[21] S. Corona-Aquino, O. Calderón-Losada, M. Y. Li-Gómez, H. Cruz-Ramirez, V. Alvarez-Venicio, M. d. P. Carreón-Castro, R. d. J. León-Montiel, and A. B. U'Ren, Experimental study on the effects of photon-pair temporal correlations in entangled two-photon absorption, arXiv:2101.10987.

[22] B. Dayan, A. Pe'er, A. A. Friesem, and Y. Silberberg, Nonlinear Interactions with an Ultrahigh Flux of Broadband Entangled Photons, Phys. Rev. Lett. **94**, 043602 (2005).

[23] A. Mikhaylov, R. N. Wilson, K. M. Parzuchowski, M. D. Mazurek, C. H. C. J. au2, M. J. Stevens, and R. Jimenez, Hot-band absorption can mimic entangled two-photon absorption, arXiv:2111.05946.

[24] T. Landes, M. Allgaier, S. Merkouche, B. J. Smith, A. H. Marcus, and M. G. Raymer, Experimental feasibility of molecular two-photon absorption with isolated time-frequency-entangled photon pairs, Phys. Rev. Res. **3**, 033154 (2021).

[25] T. Landes, M. G. Raymer, M. Allgaier, S. Merkouche, B. J. Smith, and A. H. Marcus, Quantifying the enhancement of two-photon absorption due to spectral-temporal entanglement, Opt. Express **29**, 20022 (2021).

[26] M. G. Raymer, T. Landes, M. Allgaier, S. Merkouche, B. J. Smith, and A. H. Marcus, Two-photon absorption of time-frequency-entangled photon pairs by molecules: The roles of photon-number correlations and spectral correlations, arXiv:2012.05375.

[27] J. Mertz, Ch. 5 for (4), (6) and Ch. 14 for (3), (5), in *Introduction to Optical Microscopy* (Cambridge University Press, Cambridge, England, 2019).

[28] A. Gatti, E. Brambilla, L. Caspani, O. Jedrkiewicz, and L. A. Lugiato, x Entanglement: The Nonfactorable Spatiotemporal Structure of Biphoton Correlation, Phys. Rev. Lett. **102**, 223601 (2009).

[29] N. S. Makarov, M. Drobizhev, and A. Rebane, Two-photon absorption standards in the 550–1600 nm excitation wavelength range, Opt. Express **16**, 4029 (2008).